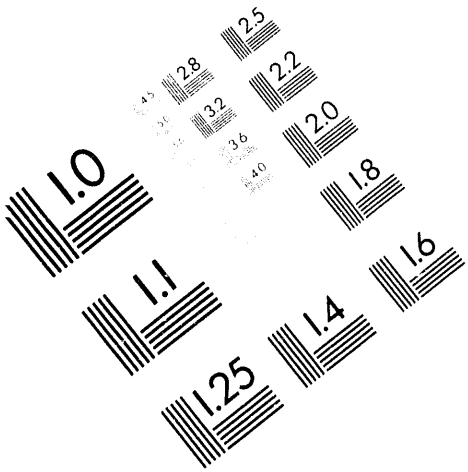

AIIM

Association for Information and Image Management

1100 Wayne Avenue, Suite 1100
Silver Spring, Maryland 20910

301/587-8202

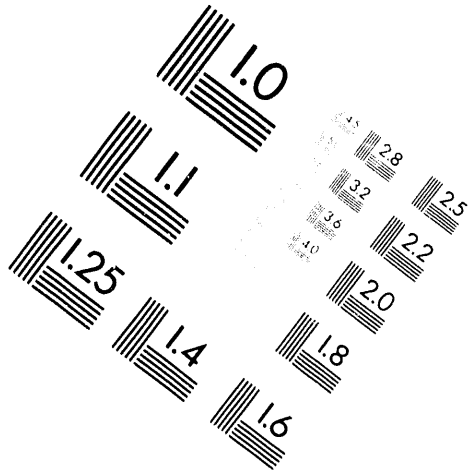

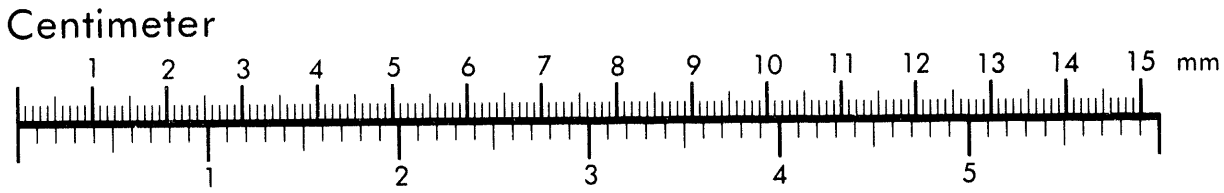

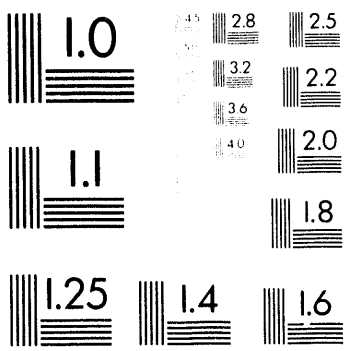

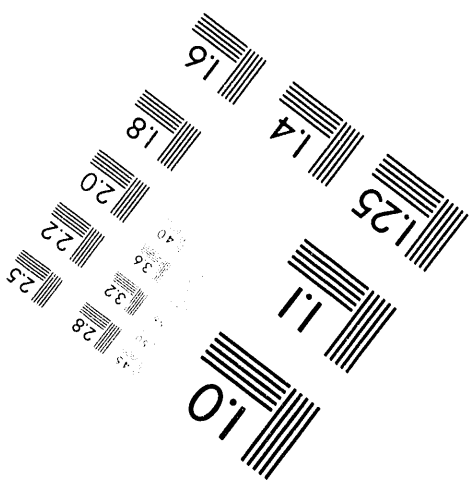

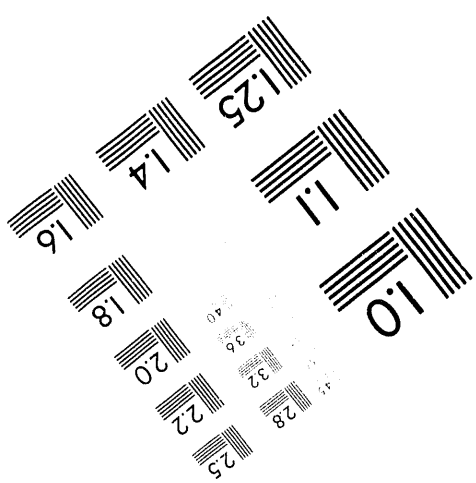

MANUFACTURED TO AIIM STANDARDS
BY APPLIED IMAGE, INC.

1 of 1

DISCLAIMER

PAPER

VALIDATION OF THE TIARA CODE TO TRITIUM INVENTORY DATA*

by

M. C. BILLONE
Fusion Power Program
Energy Technology and Technology Development Divisions
Argonne National Laboratory
Argonne, IL 60439 USA

March 1994

To be presented at the Third International Workshop on Ceramic Breeder Blanket Interactions, University of California, Los Angeles, June 22-24, 1994.

*Work supported by the United States Department of Energy/Office of Fusion Energy, under Contract No. W-31-109-Eng-38.

VALIDATION OF THE TIARA CODE TO TRITIUM INVENTORY DATA

by

Michael C. Billone
Fusion Power Program
Argonne National Laboratory
Argonne, IL 60439 USA

Abstract

The TIARA code has been developed to predict tritium inventory in Li_2O breeder ceramic and to predict purge exit flow rate and composition. Inventory predictions are based on models for bulk diffusion, surface desorption, solubility and precipitation. Parameters for these models are determined from the results of laboratory annealing studies on unirradiated and irradiated Li_2O. Inventory data from in-reactor purge flow tests are used for model improvement, fine-tuning of model parameters and validation. In this current work, the inventory measurement near the purge inlet from the BEATRIX-II thin-ring sample is used to fine tune the surface desorption model parameters for T > 470°C, and the inventory measurement near the midplane from VOM-15H is used to fine tune the moisture solubility model parameters. TIARA predictions are then validated to the remaining inventory data from EXOTIC-2 (1 point), SIBELIUS (3 axial points), VOM-15H (2 axial points), CRITIC-1 (4 axial points), BEATRIX-II thin ring (3 axial points) and BEATRIX-II thick pellet (5 radial points). Thus, of the 20 data points, two were used for fine tuning model parameters and 18 were used for validation. The inventory data span the range of 0.05 - 1.44 wppm with an average of 0.48 wppm. The data pertain to samples whose end-of-life temperatures were in the range of 490 - 1000°C. On the average, the TIARA predictions agree quite well with the data (< 0.02 wppm difference). However, the root-mean-square deviation is 0.44 wppm, mostly due to over-predictions for the SIBELIUS samples and the higher-temperature radial samples from the BEATRIX-II thick-pellet. Excellent agreement was obtained for the VOM-15H data along the stack length, and the CRITIC-1 and BEATRIX-II (thin ring) data from the lower half of the pellet stack.

Introduction

The TIARA code has been developed to predict the steady-state inventory in tritium-breeding ceramics and the gas phase distribution and flow rates of tritium species (HT, HTO, and T_2O) in the purge. Initial efforts were directed toward modeling Li_2O ceramic in the plate geometry of the ITER/CDA design.[1] Input to TIARA includes geometrical parameters, microstructural parameters (density/porosity, grain size, and specific pore/solid surface area), purge inlet parameters (helium pressure and flow rate, H_2 partial pressure, and H_2O partial pressure) and operational parameters (uniform tritium generation rate and one-dimensional temperature profile). Based on these input parameters and models for diffusion, surface desorption, solubility and precipitation (e.g. LiOH/LiOT separate phase formation), the two-dimensional (thickness direction and purge flow direction) profile of tritium inventory is calculated. Auxiliary models are also incorporated into the code to calculate a two-dimensional partial pressure profile for protium/tritium species (H_2, HT, H_2O, HTO, and T_2O) in the purge and internal interconnected porosity. In order to validate the tritium retention models and to expand code capabilities, options have been included for analysis of solid and annular cylindrical geometry.

Previous efforts[1,2] to validate TIARA have been limited by uncertainties in experimental conditions and the scarcity of tritium inventory data for Li_2O which has been irradiated in purged capsule experiments. However, the inventory database has expanded from four points at the time of Ref. 1 to nine points at the time of Ref. 2 to 20 points for the current work. Also, through extensive interaction with the experimenters, characterization of the as-fabricated parameters, of the end-of-life microstructures, and of the operating conditions has improved considerably.

While the Li_2O database has expanded, the basic methodology for TIARA development and validation has remained the same. The models developed for steady-state tritium retention include the mechanisms of diffusion, surface desorption, solubility, and precipitation. Model parameters are determined based on laboratory annealing studies of unirradiated and irradiated samples. Tritium inventories measured after the completion of in-reactor, purge-flow experiments are then used for code validation.

In the case of the desorption model, the laboratory data on porous, polycrystalline samples is limited in temperature ($T < 470°C$). One of the

measured inventories (BEATRIX-II thin ring near the purge inlet) from the in-reactor, purge-flow database is used for higher temperature (T > 470°C) extrapolation of the desorption model. For the solubility of moisture in Li_2O, two data sets are available. These data sets agree at high temperature (~1000°C), but they diverge at lower temperatures. The VOM-15H inventory measurement near the stack midplane is used to resolve the discrepancy in the two laboratory data sets. Thus, of the 20 tritium data points available from in-reactor purge-flow tests, two have been used to help set uncertain model parameters, and the remaining 18 data points are used for validation.

2. Database

2.1 Lattice Diffusivity

The diffusivity of tritium in single crystal Li_2O has been measured in three independent studies.[3,4,5] Figure 1 shows the data for the diffusion coefficient vs. inverse temperature for a range of crystal diameters and/or thicknesses (150–3200 μm) and purge gas compositions (He, He+H_2, and NH_3). The results are remarkably consistent and can be fit within a factor of two in the temperature range of 300 to 900°C by

$$D = 4.03 \times 10^{-2} \exp\left(-95.1\ \mathrm{kJ \cdot mol^{-1}} / RT\right),\ \mathrm{cm^2/s} \qquad (1)$$

where $R = 8.314 \times 10^{-3}$ kJ(mol•K)$^{-1}$.

2.2 Surface Desorption

Quanci[5] measured the rate constant for surface desorption from Li_2O. He used a post-irradiation annealing experimental technique and a very careful mathematical analysis to determine the rate constant for single crystal Li_2O and polycrystalline Li_2O (78% dense pellets with specific surface area of 1200 cm^2/g and 25 μm grain size). The annealing was performed in ultra high purity (UHP) He, He + 0.097% H_2 (107 Pa), He + 1% H_2 (1100 Pa), and He + 4.82% H_2 (5320 Pa). Quanci's data are shown in Fig. 2 in terms of the rate constant k_{eff} (in 1/s). The results have been normalized to a protium pressure of 107 Pa by assuming a square-root dependence. For the UHP case, a protium pressure of 50 Pa has been assumed for the purpose of the figure. For a first-order desorption-

dominated process and isothermal annealing, k_{eff} appears in the equation for retained tritium fraction ($f = I/I_o$) as

$$f = \exp(-k_{eff} \bullet t) \qquad (2)$$

where t is time in seconds. It is interesting to note that the higher-temperature single-crystal data are less sensitive to protium pressure and appear to have a lower activation energy than the extrapolation of the lower-temperature polycrystalline data. For modeling purposes, the parameter $k = (A_s/V)^{-1}k_{eff}$, where A_s is the pore-solid surface area for free or interconnected porosity and V is the solid volume, is needed. For the single crystals, A_s/V ranges from 30 to 50 cm^{-1} ($15 \le a_s \le 25$ cm^2/g). For the polycrystalline samples $A_s/V = 2380$ cm^{-1} ($a_s = 1200$ cm^2/g). It is not clear at this time why the two data sets are consistent in magnitude for k_{eff} rather than for k. The lowering of the activation energy in going from the polycrystalline data to the single crystal data is less problematic as there may be a change in mechanism in going from low temperature (polycrystalline data) to high temperature (single crystal data). The approach taken in the current work is to use the Quanci polycrystalline data for the low temperature ($T < 744$ K) branch of the desorption model and the BEATRIX-II data (at $X/L \sim 0$) for the high temperature branch, with the two rate constants constrained to be equal at the LiOH melting temperature (744 K). The results are shown in Fig. 2, and they are described mathematically below.

The model assumed for the surface desorption rate constant is

$$k = A \exp(-Q_d / RT) P_{H_2}^{0.5}, \text{ cm/s} \qquad (2a)$$

and

$$k_{eff} = (A_s / V)k, \text{ 1/s} \qquad (2b)$$

The best-fit correlation to polycrystalline data is the same relationship which has been used previously[1,2] to model Li_2O surface desorption:

$$k = 25.3 \exp\left(-131 \text{ kJ} \cdot \text{mol}^{-1} / RT\right) P_{H_2}^{0.5}, \text{ cm/s} \qquad (2c)$$

Also shown in Fig. 2 is the value of k_{eff} (normalized to 107 Pa and $a_s = 1200$ cm^2/g) needed to match the BEATRIX-II thin ring inventory data (0.23

wppm) at X/L ~ 0. Constraining the high temperature (T ≥ 744 K) branch of the desorption rate constant to match the BEATRIX data and Eq. 2a at T = 744 K gives A = 3.62×10^{-4} and Q = 62 kJ•mol^{-1}. Thus, the high temperature branch is described by

$$k = 3.62 \times 10^{-4} \exp\left(62\ \text{kJ} \bullet \text{mol}^{-1} / RT\right) P_{H_2}^{0.5},\ \text{cm/s} \qquad (2d)$$

The decision to use the purge–inlet BEATRIX–II data as a desorption rate data point rather than the single crystal data is motivated by two factors: the microstructure (e.g. grain size, density, specific pore/solid surface area) of the BEATRIX sample is more similar to the Quanci polycrystalline sample than the microstructure for the single crystals; and desorption is most likely rate–limiting for the BEATRIX sample near the purge inlet where the tritium partial pressure is essentially zero. The decision to match the two results at the LiOH melting temperature (744 K) is somewhat arbitrary. It is motivated by the general observation that tritium inventory tends to increase more rapidly with temperature decrease as the temperature drops below 744 K. While these motivating factors are appealing, the ultimate justification for Eqs. 2c and 2d must come from the validation to independent data sets.

2.3 Solubility

2.3.1 Li_2O/H_2O

In previous efforts,[1] the data of Tetenbaum, Fischer and Johnson[6] were used to describe the solubility of OH in Li_2O. The temperature and pressure ranges for these data are 700 ≤ T ≤ 1000°C and 3 ≤ P_{H_2O} ≤ 106 Pa, respectively. The data are given in tabular form in Ref. 6 and correlate best with $P_{H_2O}^{0.5}$. The data, normalized to $P_{H_2O}^{0.5}$, are plotted in Fig. 3. Also shown in Fig. 3 are the data of Hightower and Norman[7] in the temperature and H_2O partial pressure ranges of 512 to 977°C and 2 to 90 Pa, respectively. The points in Fig. 3 are taken from the graphical representations in Ref. 7. Notice that there is considerable scatter within each data set and a divergence in results as temperature decreases.

In order to resolve the discrepancy in moisture solubility data and select one correlation for moisture solubility, S_{OH}, the tritium retention measurements from near the midplane of VOM–15H were considered. VOM–15H was irradiated at an average end–of–life temperature of 732°C

with no protium purging. Thus, solubility is anticipated to be the dominant retention mechanism, and HTO is predicted to be the dominant tritiated gas species. The calculated H/T ratio at the purge outlet is ~1 (0.9±0.6) based on typical levels of H_2O impurities in the purge. The range of solubility values needed to match the VOM-15H tritium inventory data for assumed moisture impurity levels of 0.3±0.2 vppm in the He purge is shown in Fig. 3. Fitting the average of these points along with the intersection of the TFJ and NH correlations gives:

$$S_{OH} = 6.47 \times 10^3 \exp\left(-51\ \text{kJ} \bullet \text{mol}^{-1} / RT\right) P_{H_2O}^{0.5},\ \text{mppm} \qquad (3a)$$

where wppm means moles of OH per million moles of Li_2O. This procedure insures consistency with the two solubility data bases while giving good results for VOM-15H.

2.3.2 Li_2O/H_2

The data of Kudo et al.[8] are shown in Fig. 4 for single crystal and powder samples. Only the low H_2 (really T_2 and H_2/HT) partial pressures (≤ 300 Pa) are shown and used for the derivation of the correlation. The single crystal results for the hydrogen solubility, S_H, are clearly lower than the powder results. Because the powdered sample has grain size and surface area closer to the validation samples than the single crystals, these data are used to develop the solubility correlation:

$$S_H = 118.5 \exp\left(-21.4\ \text{kJ} \bullet \text{mol}^{-1} / RT\right) P_{H_2}^{0.5} \qquad (3b)$$

2.3.3 Comparison of Li_2O/H_2O and Li_2O/H_2 results

Figure 4 shows the comparison of the hydrogen solubilities for the Li_2O/H_2O and Li_2O/H_2 systems, normalized to the square-root of the respective gas pressures. As the chemical form of the dissolved hydrogen is most likely OH- in both cases, intuitively one would expect higher solubility for the moisture case than for the reduced case. The correlations are consistent with this logic for T > ~600°C. However, the curves cross for lower temperatures. Notice that the solid lines in Fig. 5 represent the temperature range for the databases of each system. Thus, the lower temperature extrapolation of the moisture solubility curve is what crosses the reduced form solubility data curve. Given the scatter in the moisture

solubility data and the uncertainty in the extrapolation, this crossing is not significant. Also, given the probable amounts of moisture absorbed to the as-fabricated powder surfaces, as well as the moisture impurities in the purge, both types of experiments may be giving the same results for T < 600°C. The implication of this is that Eq. 3b may predict too high of a solubility for long-time experiments in which the initial moisture content of the Li_2O may be released due to long-time exposure to a protium-rich and oxygen-poor purge. Until more controlled data sets become available, the validation exercise may be used to resolve, at least partially, this issue.

2.4 In-Reactor, Purge-Flow Experimental Database

Table 1 summarizes the mass, geometry, microstructure, and operating conditions for the EXOTIC-2[9,10], SIBELIUS[11,12], VOM-15H[13,14], CRITIC-1[15,16], BEATRIX-II (thin-ring)[17-20], and BEATRIX-II (thick ring)[17,19,20] Li_2O samples. Values in parentheses are estimated. Notice that the specific pore/solid surface area, which is important to the desorption model, is generally not measured either before or after the experiment. Based on the BEATRIX-II thin-ring measurement of 0.06 m^2/g for 80% dense Li_2O, as well as the MOZART[21] measurement of 0.05 m^2/g and the Quanci[5] measurement of 1200 m^2/g, it appears that a reasonable range for this parameter is 0.05 -0.12 m^2/g for 80% dense Li_2O. Higher densities and/or larger initial powder size would tend to produce lower values. Similarly, with the exception of the CRITIC-1 experiment, the amount of open or interconnected porosity is generally not characterized. For these cases, the experimental results of Takahashi and Kikuchi[22] are used to estimate the fraction of as-fabricated porosity which is open.

With regard to operating conditions, the purge flow and chemistry conditions are well characterized. The tritium generation rates are determined by comparison with calculated tritium generation rates, measured tritium release, and/or measured burnup. The values in Table 1 are meant to represent spatially-averaged values near the end of the irradiation. Considering calculational and experimental uncertainties, as well as axial and radial variations, the error in these estimates is on the order of ±10%. For the temperature distribution across the sample, at least one temperature (e.g., hot inner temperature) is generally measured and the other one (e.g., cold outer temperature) is calculated. The heat generation rates listed in Table 1 are not used directly in this current work. They are simply inferred from the quoted inner/outer temperatures and a one-

dimensional heat transfer analysis. Because of the short lengths of the pellet stacks (as compared with typical fission-reactor fuel elements), two-dimensional heat transfer will be significant near the ends of these experimental samples. Thus, the temperatures listed pertain to the midplane of the sample stack. Temperatures at the lower and upper end of the stack may tend to be lower.

Table 2 lists the inventory measurements, along with the approximate radial and axial locations for the measurements. These measurements were performed in the laboratory by a variety of annealing and dissolution techniques. They are considered to be much more reliable than those obtained indirectly from in-reactor transient release data or from post-irradiation annealing of samples in-reactor with long purge lines. From a model validation perspective, the uncertainty in these data is small relative to the uncertainty in the axial and radial location, as well as the end-of-life microstructure and operating temperatures, of the samples. Also shown in Table 2 are the predicted inventories which are discussed in a subsequent section.

Figure 6 shows an Arrhenius representation of the inventory data (normalized to the tritium generation rate) vs. inverse temperature. The ratio of inventory to generation rate is often called the tritium residency time. Prior to the generation of the inventory data in Table 2, transient release data (such as the MOZART data[21]) were used to determine residency time. Figure 6 shows the residency time correlation developed several years ago for the ITER/CDA effort[23] based on the MOZART data. The high activation energy correlation results in very low calculated inventories for T > 500°C. However, with the new database of directly measured inventories, a more reasonable bounding design correlation may be developed for a narrow range of microstructures (80–86% dense) and purge conditions (He at 0.1 liters/min with 0.1% protium). The new design correlation for residency time is:

$$\tau = \exp\left(-8.45 + 56\ \mathrm{kJ \bullet mole^{-1}} / \mathrm{RT}\right), \text{ hours} \qquad (4)$$

Equation 4 is useful in two ways. First it can be used directly by designers to obtain an easy, quick estimate of tritium inventory as a function of generation rate and temperature. Secondly, as there is no fundamental modeling involved in generating Eq. 4, it becomes a useful yardstick for model validation. While modeling based on fundamental mechanisms has

the advantage over Eq. 4 of allowing extrapolation to microstructures and operating conditions outside the range of validity of Eq. 4, it should validate to the narrow database for Eq. 4 at least as well as the simple correlation itself.

3. Models: Formulation and Assumptions

The formulation of the mathematical models and assumptions for TIARA are documented in detail in Ref. 1. They are reviewed briefly here for the convenience of the reader. It is assumed that an experimental sample and a small design element can be characterized by a uniform generation rate and a one-dimensional temperature profile. For steady-state analysis, the inventory components for diffusion, desorption, and solubility can be calculated from decoupled models for each phenomenon. The diffusive component (I_{dif} in wppm) is calculated from the relationship:

$$I_{dif}(\eta) = \left[ga^2(\eta)\right]\left[15D_o\right]^{-1} \exp\left[Q_{dif} / RT(\eta)\right] \qquad (5)$$

where g is the local generation rate in wppm/s, a is the grain radius in cm, $D_o = 4.03 \times 10^{-2}$ cm^2/s (from Eq. 1), $Q_{dif} = 95.1$ kJ•mol^{-1} (from Eq. 1), R = 8.314×10^{-3} kJ•(mol•K)$^{-1}$, T is the local temperature in K, and η is the square of the normalized radius ($\eta = r^2/r_o^2$ for a solid cylinder of outer radius r_o and $n = r^2/r_i^2$ for an annular cylinder of inner radius r_i). For cylindrical geometry, the temperature distributions are given by

$$T = T_{max}\ (1 - \eta) \text{ for solid cylinder} \qquad (5a)$$

and

$$T = T_{max}\ [1 - A\ (\eta - 1 - \ln\ \eta)] \text{ for annular cylinder} \qquad (5b)$$

The local inventory (I_{des} in wppm) associated with surface desorption in the form of HTO with purge protium present is:

$$I_{des}(\eta, \xi) = g \bullet \left[a_s(\eta) \bullet \rho_{th} \bullet P_{H_2}^{0.5}(\eta, \xi) \bullet k_o\right]^{-1} \exp\left[Q_{des} / RT(\eta)\right] \qquad (6)$$

where a_s is the specific pore/solid surface area for open porosity, ρ_{th} is the theoretical density in g/cm^3, P_{H_2} is the local protium pressure in Pa, ξ is the normalized axial position (x/L) in the direction of the purge flow, k_o = 25.3 for $T \leq 744$ K and 3.62×10^{-4} for $T > 744$ (from Eqs. 2c and 2d), and

Q_{des} = 131 kJ•mol^{-1} for T ≤ 744 K and 62 kJ•mol^{-1} for T > 744 K (from Eqs. 2c and 2d).

The solubility inventory (I_{sol} in wppm) is derived from Eqs. 3a and 3b to be

$$I_{sol}(\eta,\xi) = A_{OH} \exp\left[-Q_{OH}/RT(\eta)\right] P_{T_2O}^{0.5}(\eta,\xi) + A_H \exp\left[-Q_H/RT(\eta)\right] P_{T_2}^{0.5}(\eta,\xi) \quad (7a)$$

or

$$I_{sol}(\eta,\xi) = 0.5 \bullet A_{OH} \exp\left[-Q_{OH}/RT(\eta)\right] P_{HTO}(\eta,\xi) \bullet P_{H_2O}^{-0.5}(\eta,\xi) + 0.5 \bullet A_H \exp\left[-Q_H/RT(\eta)\right] P_{HT}(\eta,\xi) \bullet P_{H_2}^{-0.5}(\eta,\xi) \quad (7b)$$

where A_{OH} and Q_{OH} are 6.47x10^3 and 51 kJ•mol^{-1}, respectively (from Eq. 3a), A_H and Q_H are 1.185x10^2 and 21.4 kJ•mol^{-1}, respectively (from Eq. 3b).

In addition to the models for diffusion, desorption, and solubility, auxiliary models have been developed to describe the distribution of gaseous phases in the interconnected porosity and the purge. These are described in Ref. 1. In order to apply these relationships to the in-reactor purge-flow cases, it is assumed that the H, T, and O species come to equilibrium in the purge flow gas at the purge flow temperature. In order to calculate the increase in tritium pressure across the interconnected porosity, it is assumed that the ratios of HT/HTO and HT/T_2O in the open porosity are equal to those in the purge at that axial location. Gas-phase diffusion of these species from the interior open porosity to the purge is then assumed to occur independently in order to calculate the HT and HTO partial pressure increases from the purge to the interior of the breeder. With regard to the first assumption, the temperature gradient across each sample, with the exception of the BEATRIX-II thick-pellet case, is small, and calculated results show little sensitivity to the equilibrium-temperature assumption. It is difficult to test the second assumption because partial pressure increases across the samples are small.

4. Validation Results

The TIARA validation results are summarized in Table 2 and Fig. 7. For all 20 cases, the diffusive component of the inventory is calculated to be small compared to the measured inventory. The EXOTIC-2 case has a low tritium generation rate, a high H/T ratio, and a moderate temperature. The desorption component is calculated to dominate solubility for this case. Both the calculated and measured inventories are small (<0.1 wppm). Although the calculated inventory is about one-half of the measured inventory, this is considered acceptable agreement for such low tritium concentrations. For SIBELIUS, the higher generation rate, the lower temperature and the lower protium pressure in the purge drive the desorption inventory predictions up to ~0.5 wppm, while the measured inventories are ~0.1 wppm. It is not clear why the measured SIBELIUS inventory is not much greater than the EXOTIC-2 inventory. Closer agreement between predictions and data would be obtained for SIBELIUS if the hydrogen pressure (obtained from the estimated helium system pressure) were higher and/or the generation rate were lower than calculated.

The agreement between TIARA predictions and data are excellent for the three VOM-15H data points. Recall that the average of these points was used to fine tune the moisture solubility model. Figure 8a shows the predicted rise in inventory along the purge flow axis, as compared to the data. The agreement is quite good both in terms of average prediction and axial profile. As moisture solubility should be the dominant tritium retention mechanism for this temperature range with no protium added to the purge, these results validate the use of Eq. 3a for OH/OT solubility in Li_2O in response to low levels of moisture pressure.

The TIARA comparison to CRITIC-1 and BEATRIX-II (thin-ring) data shows the same trends. Using the thin-ring data point near the purge inlet to fine-tune the desorption model for T > 471°C results in very good agreement with the data for X/L < 0.4 (see Fig. 8b). Above that axial location, the rise in measured rise in inventory is much greater than predicted. Within the context of the models and model parameters used for the validation, the results would agree better with the data if the HT and HTO partial pressures were higher than predicted by equilibrium considerations for these cases in which the H/T ratio is moderate (50 - 100).

The BEATRIX-II thick-pellet results are summarized in Fig. 9, as well as in Table 2 and Fig. 7. The agreement with the data at the farthest radial position is good considering the uncertainty in radial position for the data, the uncertainty in temperature, and the steep rise in predicted values as the outer radius is approached. The major discrepancy (order of magnitude higher prediction) is with the four inner data points which are at T > 564°C. Both the calculated solubility component and the calculated surface desorption component are higher than the measurements. Also, as the data give a relatively flat profile, the uncertainty in radial location is not important. These points were measured in the columnar and equiaxed zones which are characterized by large grains and high density. In principle, the pore/solid surface areas for these regions should be small, which drives up the surface desorption prediction. Also, the temperature is relatively high and the H/T ratio is moderate. Both of these factors explain the relatively large solubility component predicted. Thus, within the context of the models chosen and the model parameters used, it is difficult to resolve the discrepancy. However, the discrepancy is consistent with the spread in laboratory data for single crystals as compared to porous polycrystalline samples. Figures 2 and 4 show single-crystal data, as well as porous, polycrystalline data. The measured desorption rate for single crystals is much higher than what would be predicted by the porous model when the free surface area is used for scaling. For Quanci's porous pellets, the specific surface area was 1200 cm^2/g, while the single crystals had a specific free surface area of only ~20 cm^2/g. Model predictions obtained by scaling the effective desorption rate by the specific surface area (factor of 600 decrease) are in disagreement with the single-crystal desorption data, as well as the data from the dense columnar and equiaxed regions of the BEATRIX-II thick pellet. Similarly, single-crystal data for the Li_2O/H_2 system give about an order of magnitude decrease in solubility as compared to the powder results. The major difference for these samples is again the specific free surface area. These results suggest that the validity of the model parameters may be restricted in terms of density and specific free surface area.

In the current validation effort, only 2 inventory data points were used to "fine tune" or "calibrate" model parameters. The resulting model parameters were held fixed during the validation to the other 18 data points. This exercise is quite different from a "best-fit" approach in which all of the data are used to help set model parameters. It is interesting to note that the results in Table 2 and Fig. 7 are in excellent agreement with

the average of the measured inventories (0.48 wppm). However, the standard deviation between predictions and data is relatively high (0.44 wppm), mostly due to the SIBELIUS results and the higher temperature BEATRIX-II thick-pellet results.

5. Discussion

The progress in developing correlations, models, and codes for predicting the steady-state tritium inventory in Li_2O has come largely from the expansion of the tritium inventory database, the postirradiation characterization of sample microstructure, and the improvement in quantifying as-fabricated parameters and operating conditions. Thus, while the fundamental models have remained basically the same over the past five years, the quantification of model parameters (e.g., pre-exponentials and activation energies) has improved with the use of both laboratory annealing studies and postirradiation inventory measurements.

The inventory data may be used directly (see Fig. 6) within a narrow range of microstructures (e.g., 80-86 % TD, 10-200 μm grain size) and protium purge concentrations (e.g., 100-300 Pa protium inlet pressure and outlet protium/tritium ratios ≥ 40) to develop a correlation for tritium residency time. Implicit in this approach is a one-mechanism model which may be used for fast, easy design estimates of tritium inventory within a narrow range of design conditions. In modeling terminology, this represents a "zeroeth-order" approach. The approach used in the current work is "first-order" in terms of sophistication in that relatively simple models are proposed for basic mechanisms (diffusion, surface desorption, and solubility), but activation energies and pre-exponentials are chosen based on data rather than on fundamental principles. Reasonable success has been achieved with this approach in modeling the steady-state tritium inventory in Li_2O. For the 18 validation cases which cover a wide range of generation rates, temperatures, microstructures, and protium purge levels, the average of the predictions is in excellent agreement with the average of the data. This was achieved with no additional adjustment of model parameters. However, even this "first-order" approach to modeling may have a limited range of validity in terms of microstructures and operating conditions. The TIARA code predicted higher inventories (~0.6 wppm) than measured (~0.06 wppm) for the dense (92-96% TD), large-grain-size (200-1500 μm) regions of the BEATRIX-II thick-pellet case. While both

the measurements and the predictions are small in a design sense, they may be important from a modeling perspective.

In order to compare the tritium residency time approach to the TIARA approach, the TIARA validation results are superimposed on Fig. 6 and shown in Fig. 9. The horizontal scale has been changed from a 1/T scale to a T scale in Fig. 9 for illustrative purposes. Also, only points derived from inventory measurements are shown. Within a narrow range of operating conditions (80–86% density and 0.1% H_2 in 0.1 liters/min purge), the simple design correlation does as good a job in bounding the data as the TIARA code does in fitting the data. The primary advantage of TIARA over the simple design correlation is in its ability to extrapolate to lower hydrogen levels (0–0.01% H_2), as well as providing a detailed description of the partial pressures and flow rates of tritium species exiting the breeder. Also, it is not clear whether or not the simple design correlation extrapolates well to higher tritium generation rates which, in turn, reduce the H/T ratio for fixed purge flow rate and chemistry.

In summary, the bounding design approach of determining steady-state inventory by the use of a tritium residency time correlation does a very good job of providing a reasonable upper bound on the inventory within a narrow range of as-fabricated microstructures, purge flow rates and chemistry conditions, and tritium generation rates. The TIARA predictions provide more of a best-estimate approach for calculating tritium inventory over a wider range of as-fabricated microstructures and purge-flow chemistries. There is also good reason to believe that the more-fundamentally correct TIARA approach will give a better extrapolation in terms of purge flow rate and tritium generation rate. In addition, TIARA predicts the distribution of tritiated species at the purge exit from the breeder. This information is important for tritium processing. TIARA also predicts the form and distribution of the retained tritium. Such information is important in the breeder safety analysis in the event of overheating transients.

6. Conclusions

Significant progress has been made over the past several years in determining model parameters and improving the predictive capability of the TIARA code because of the expansion of the tritium inventory database and the better quantification of experimental conditions. Baseline parameters for the diffusion, surface desorption, and solubility models were

first determined form well-controlled laboratory annealing studies of unirradiated and irradiated Li_2O. In the case of lattice or bulk diffusivity, three independent data sets for single crystals produced very consistent results. The laboratory database for surface desorption from porous, polycrystalline samples is limited to $T \leq 470°C$. Single crystal results and one of the measured inventories from the BEATRIX-II thin-ring pellets were used to determine desorption model parameters for $T > 470°C$. The two laboratory databases for hydrogen solubility in the Li_2O/H_2O system showed agreement for $T \sim 1000°C$, but divergence at lower temperatures. One of the VOM-15H tritium inventory data points was used to determine an effective activation energy for extrapolation to temperatures $< 1000°C$. With model parameters fixed, the remaining 18 tritium inventory data points measured after in-reactor, purge-flow testing were used to validate the TIARA code. The average of the TIARA predictions is in excellent agreement with the average (0.48 wppm) of the data. However, the standard deviation of the predictions as compared to the data is high (±0.44 wppm) relative to the mean mostly because of over-predictions for the tritium inventory in the dense, large-grain-size, high temperature regions of the BEATRIX-II thick pellet. Similar discrepancies between model predictions and data were observed for laboratory studies of desorption and solubility in large single crystals. While the TIARA models appear to be adequate for predicting steady-state inventory as a function of temperature, tritium generation rate, purge flow rates and chemistry, and as-fabricated microstructures characteristic of current design conditions, a more fundamental approach may be needed for basic materials studies to allow extrapolation to larger (> 100 μm) grain sizes and higher (> 91%) densities.

References

1. M. C. Billone, H. Attaya, and J. P. Kopasz, "Modeling of Tritium Behavior in Li_2O," Argonne National Laboratory Report ANL/FPP/TM-260 (August 1992).

2. M. C. Billone and I. Gomes, "Validation of the TIARA Code to BEATRIX-II Li_2O Inventory Data," Proceedings of the International Workshop on Ceramic Breeder Blanket Interactions, Commissariat à l'Energie Atomique, Paris, France, September 22-24, 1993 (January 1994), pp. 105-130.

3. D. Guggi, H. R. Ihle, D. Brüning, and U. Kurz, "Diffusion of Tritium in Single Crystal Li_2O," J. Nucl. Mater. 118 (1983) 100.

4. T. Tanifuji, K. Noda, T. Takahashi, and H. Watanabe, "Tritium Release from Neutron Irradiated Li_2O: Diffusion in Single Crystal," J. Nucl. Mater. 149 (1987) 227.

5. J. F. Quanci, "Tritium Breeding and Release–Rate Kinetics from Neutron–Irradiated Lithium Oxide," Ph.D. dissertation, Princeton University, Princeton, NJ (January 1989).

6. M. Tetenbaum, A. K. Fischer, and C. E. Johnson, "An Investigation of the Solubility of LiOH in Solid Li_2O," Fusion Tech. 7 (1985) 53.

7. J. H. Norman and G. R. Hightower, "Measurements of the Activity Coefficient of LiOH Dissolved in Li_2O (s) for an Evaluation of Li_2O as a Tritium Breeding Material," J. Nucl. Mater. 122 + 123 (1984) 913.

8. H. Kudo, S. O'Hira, M. Fujie, and K. Noda, "Interaction of Tritium Gas with Li_2O Crystals," J. Nucl. Mater. 179–181 (1991) 800.

9. H. Kwast, R. Conrad, L. Debarberis, A. J. Flipot, P. Kennedy, and J. D. Elen, "Tritium Release from the Various Solid Breeder Materials Irradiated in EXOTIC Experiments 1, 2, and 3" J. Nucl. Mater. 155–157 (1988) 558–562.

10. H. Kwast, personal communication, ECN, November 9, 1993.

11. W. Dienst, D. Schild, and H. Werle, "Tritium Release of Li_4SiO_4, Li_2O and Beryllium and Chemical Compatibility of Beryllium with Li_4SiO_4, Li_2O and Steel (SIBELIUS Irradiation)," KfK 5109, December 1992.

12. J. P. Kopasz, personal communication, ANL, November 10, 1993.

13. T. Kurasawa, H. Yoshida, H. Takeshita, H. Watanabe, T. Miyauchi, T. Matui, H. Umei, and Y. Naruse, "In Situ Tritium Recovery Experiment from Lithium Oxide under High Neutron Fluence," J. Nucl. Mater. 133–134 (1985) 196–200.

14. T. Kurasawa, personal communication, JAERI, December 22, 1993.

15. R. A. Verrall, J. M. Miller, I. J. Hastings, D. S. MacDonald, and D. H. Rose, "CRITIC-I - Tritium Release and Post-Irradiation Examination of Large-Grained Lithium Oxide," Fabrication and Properties of Lithium Ceramics II, American Ceramics Soc., Inc., Westerville, OH (1990) 299.

16. R. A. Verrall, personal communication, AECL (Chalk River), March 18, 1994.

17. O. D. Slagle, K. Noda, and T. Takahashi, "Fabrication of Lithium Ceramic Pellets, Rings, and Single Crystals for Irradiation in BEATRIX-II, Advances in Ceramics: Fabrication and Properties of Lithium Ceramics, Vol. 27, ed. by G. W. Hollenberg and I. J. Hastings (1990) 77-93.

18. O. D. Slagle, T. Kurasawa, R. A. Verrall, and G. W. Hollenberg, "In-Situ Tritium Recovery from Li_2O Irradiated in Fast Neutron Flux - BEATRIX-II Temperature Change Specimen," J. Nucl. Mater. 191-194 (1992) 214-218.

19. O. D. Slagle, T. Takahashi, F. D. Hobbs, K. Noda, D. L. Baldwin, G. W. Hollenberg, and R. A. Verrall, "Postirradiation Examination of BEATRIX-II, Phase 1," to published in the proceedings of ICFRM-6, Stresa, Italy, Sept. 27-Oct. 1, 1993.

20. O. D. Slagle, personal communication, PNL, February 2, 1994.

21. C. E. Johnson, M. Masson, N. Roux, and H. Watanabe, "The MOZART Experiment: In-Pile Tritium Extraction from Lithium Oxide, Aluminates, Zirconates," Proc. 15th Symposium on Fusion Technology (SOFT), Sept. 19-23, 1988.

22. T. Takahashi and T. Kikuchi, J. Nucl. Mater. 91 (1980) 610.

23. M. C. Billone, W. Dienst, T. Flament, P. Lorenzetto, K. Noda, and N. Roux, "ITER Solid Breeder Blanket Materials Database," Argonne National Laboratory Report ANL/FPP/TM-263 (November 1993).

Table 1. Summary of Operating Conditions and Post-Irradiation Data for Tritium Inventory in Li_2O upon Completion of In-Reactor Purge Flow Experiments. Estimated Values are in Parentheses.

					BEATRIX-II (Phase 1)	
Parameter	EXOTIC-2	SIBELIUS	VOM-15H	CRITIC-1	Thin Ring	Solid Pellet
Li_2O mass, g	17.4	0.50 0.63	6.665	103	11.95	34.31
^6Li enrichment, at. %	0.6	1.93	7.42	1.78	61	61
Density, % TD BOL EOL	79.6 (79.6)	80 (80)	86±2 (86)	91±1 ~83	80 72	86.7 (87)-96
Grain size, μm BOL EOL	7.5±2.5 (10)	(20) (20)	2±1 10	55±5 55±5	5.5 10	25-40 25-1500
Inner/outer radii, mm BOL EOL	0/5 (0/5)	0/4 (0/4)	0.9/5.5 (0.9/5.5)	15/20 (15/20)	7.55/9.20 7.38/9.20	0/8.51 2.3/8.51
Spec. surf. area, m^2/g BOL EOL	(0.05) (0.05)	(0.05) (0.05)	(0.05) (0.05)	(0.015) (0.015)	0.06 (≥0.06)	(0.05) (0.015-0.05)
Open porosity, % BOL EOL	20 (20)	(18) (18)	(12) (12)	3 5-10	(18) (18)	(11) (1-11)

Table 1. Summary of Operating Conditions and Post-Irradiation Data for Tritium Inventory in Li_2O upon Completion of In-Reactor Purge Flow Experiments. Estimated Values are in Parentheses. (Continued)

					BEATRIX-II (Phase 1)	
Parameter	EXOTIC-2	SIBELIUS	VOM-15H	CRITIC-1	Thin Ring	Solid Pellet
Purge flow rate, liters(STP)/min.	0.1	0.1	0.1	0.1	0.1	0.1
Inlet purge press., Pa He H_2 H_2O	 3.0E5 300 (0.5)	 (1.0E5) (100) (0.2)	 1.6E5 ~0 0.3±0.2	 1.0E5 10 40	 2.5E5 250 (0.3)	 2.5E5 250 (0.3)
H/T ratio	670	4360 4230	~1	53	100	40
Tritium gen. rate, wppm/s	3.9E-5	2.03E-4 1.67E-4	1.4E-4	4.1E-5	3.81E-4	3.34E-4
Heat gen. rate, $W/g(Li_2O)$	(54.0)	--- (131)	(76.2)	(53.5)	72.4	65.9
Li_2O inner/outer temperature, °C	660/620	557/550 550/495	760/700	600/530	640/600	1000/450
Li_2O burnup, at.%	0.08	0.8	0.24	1.0	4.7	4.2

Table 2. TIARA Validation Results

				I (Model), wppm				
Experiment	$\bar{T}$,°C	X/L	r/r_o	Diff.	Desorp.	Solubility	Total	I (Data), wppm
EXOTIC-2	640	~0.5	Avg.	4.52E-6	0.0217	2.81E-3	0.0245	0.05
SIBELIUS	554	0.25±0.25	Avg.	3.44E-4	0.4580	1.00E-3	0.4593	0.20
	554	0.75±0.25	Avg.	3.44E-4	0.4580	1.05E-3	0.4594	0.064
	523	~0.7	Avg.	5.09E-4	0.5470	1.07E-3	0.5486	0.20
VOM-15H	732	0.38±0.12	Avg.	5.22E-6	0.0915	0.486	0.4855	0.50
	732	0.63±0.12	Avg.	5.22E-6	0.0915	0.629	0.7205	0.56
	732	0.88±0.12	Avg.	5.22E-6	0.0915	0.750	0.7495	0.94
CRITIC-1	574	0.17±0.17	Avg.	4.00E-4	0.3599	0.0172	0.3775	0.38
	574	0.50±0.03	Avg.	4.00E-4	0.3599	0.0436	0.4029	0.93
	574	0.85±0.03	Avg.	4.00E-4	0.3599	0.0758	0.4361	1.66
	574	0.97±0.03	Avg.	4.00E-4	0.3599	0.0876	0.4479	0.93
BEATRIX-2 (Thin Ring)	626	0.05±0.05	Avg.	5.40E-5	0.2299	7.33E-3	0.2373	0.23
	626	0.25±0.12	Avg.	5.40E-5	0.2299	0.0300	0.2600	0.26
	626	0.75±0.12	Avg.	5.40E-5	0.2299	0.0864	0.3164	0.44
	626	0.95±0.05	Avg.	5.40E-5	0.2299	0.1076	0.3376	0.61
BEATRIX-2 (Solid Pellet)	955	~0.4	0.37±0.10	6.15E-4	0.0863	0.4870	0.5739	0.062
	860	~0.4	0.56±0.06	1.38E-3	0.1459	0.3731	0.5204	0.069
	758	~0.4	0.70±0.06	3.83E-3	0.2828	0.2676	0.5542	0.063
	624	~0.4	0.84±0.06	5.74E-3	0.4434	0.1609	0.6100	0.056
	515	~0.4	0.94±0.02	2.92E-3	0.7777	0.0900	0.8706	1.44

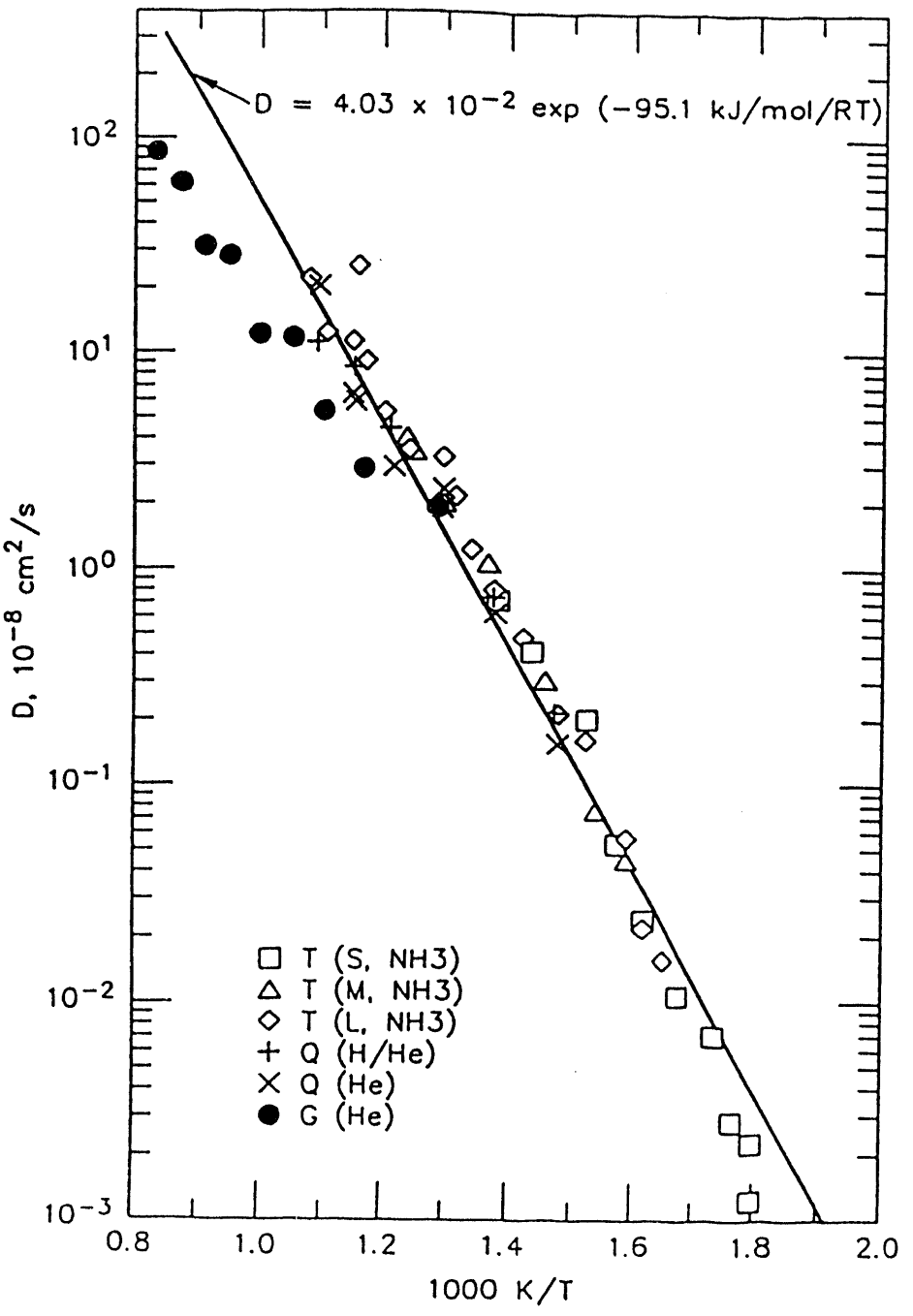

Fig. 1. Lattice diffusion coefficient for lightly-irradiated Li_2O from Tanifuji (T), Quanci (Q) and Guggi (G).

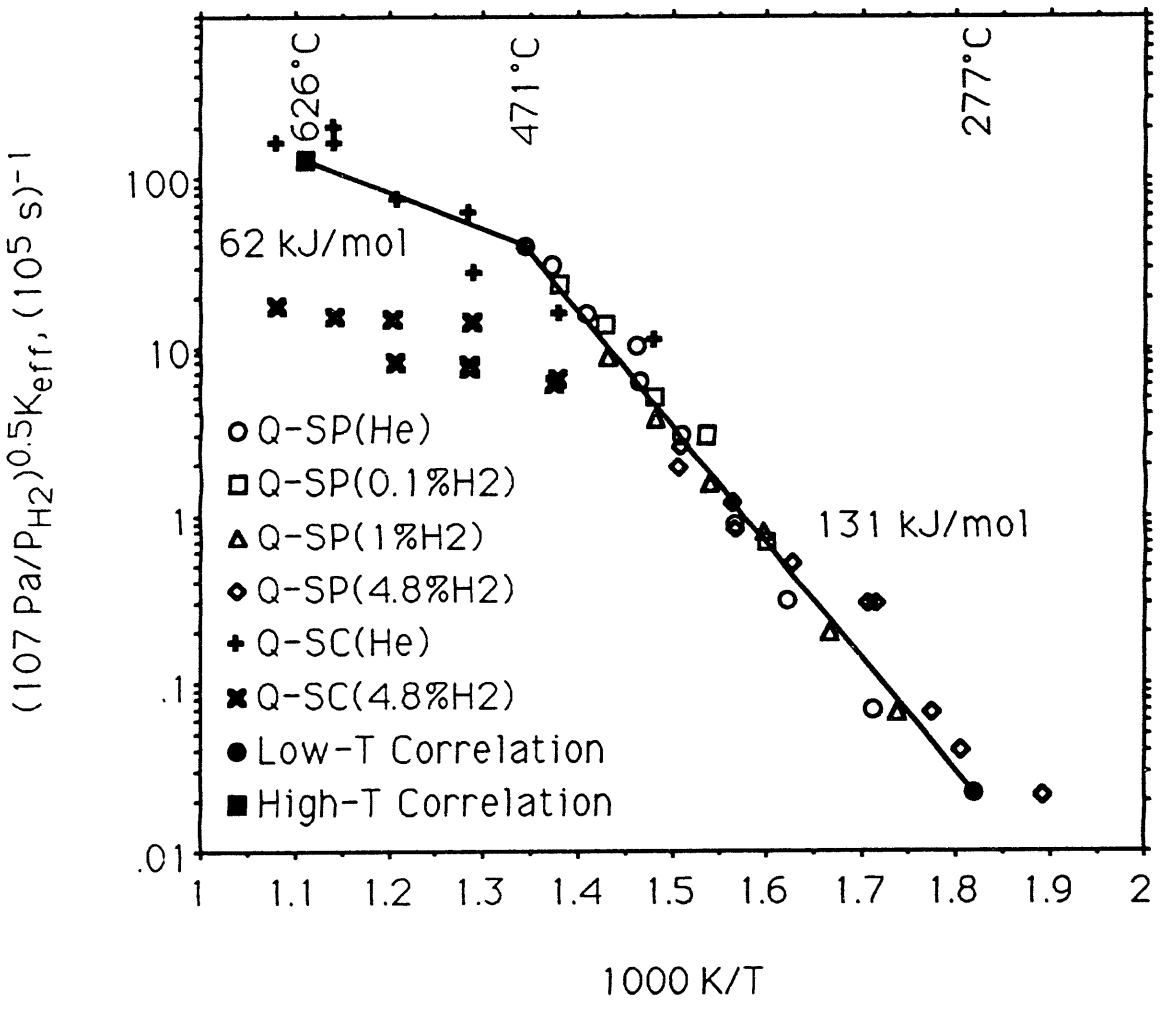

Fig. 2. Correlation vs. data for tritium desorption (from Li_2O) effective rate constant.

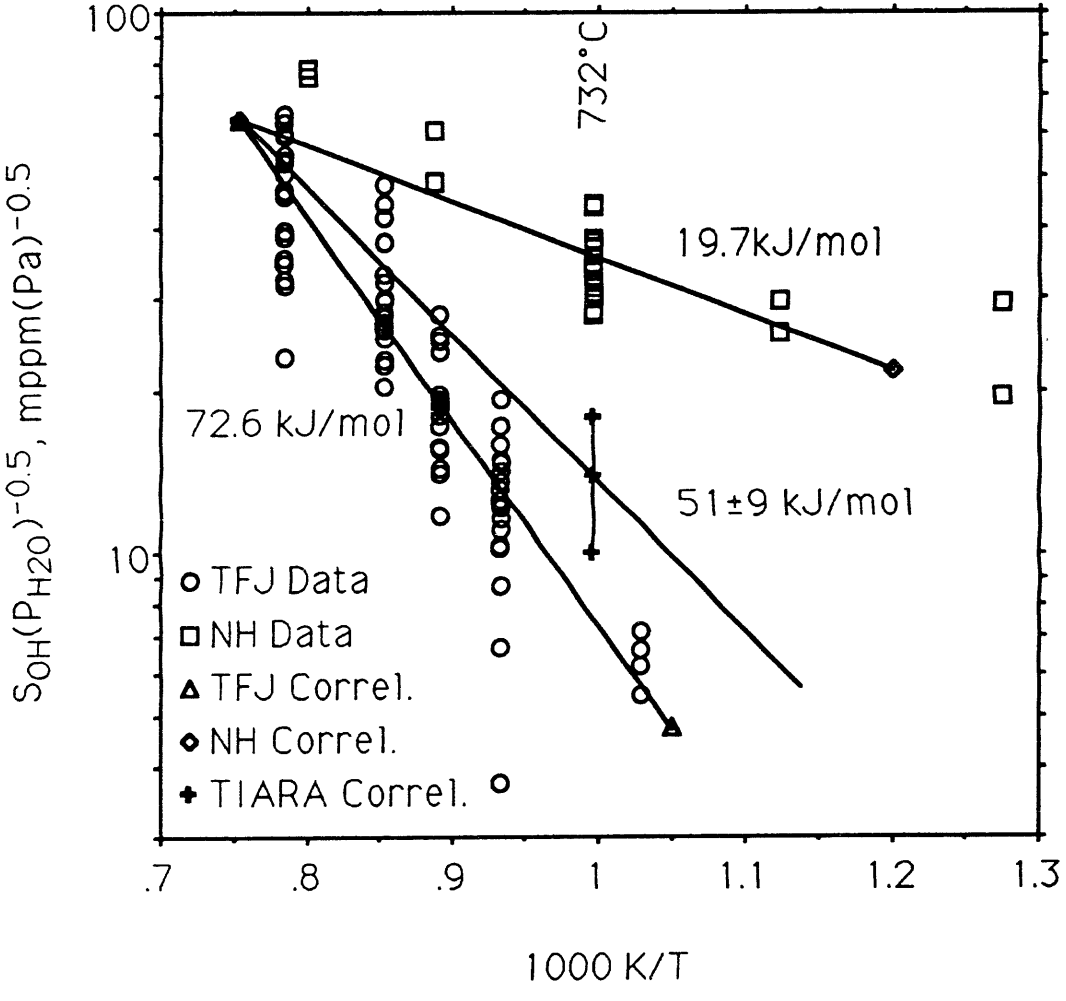

Fig. 3. Correlation vs. data for normalized OH solubility in Li_2O.

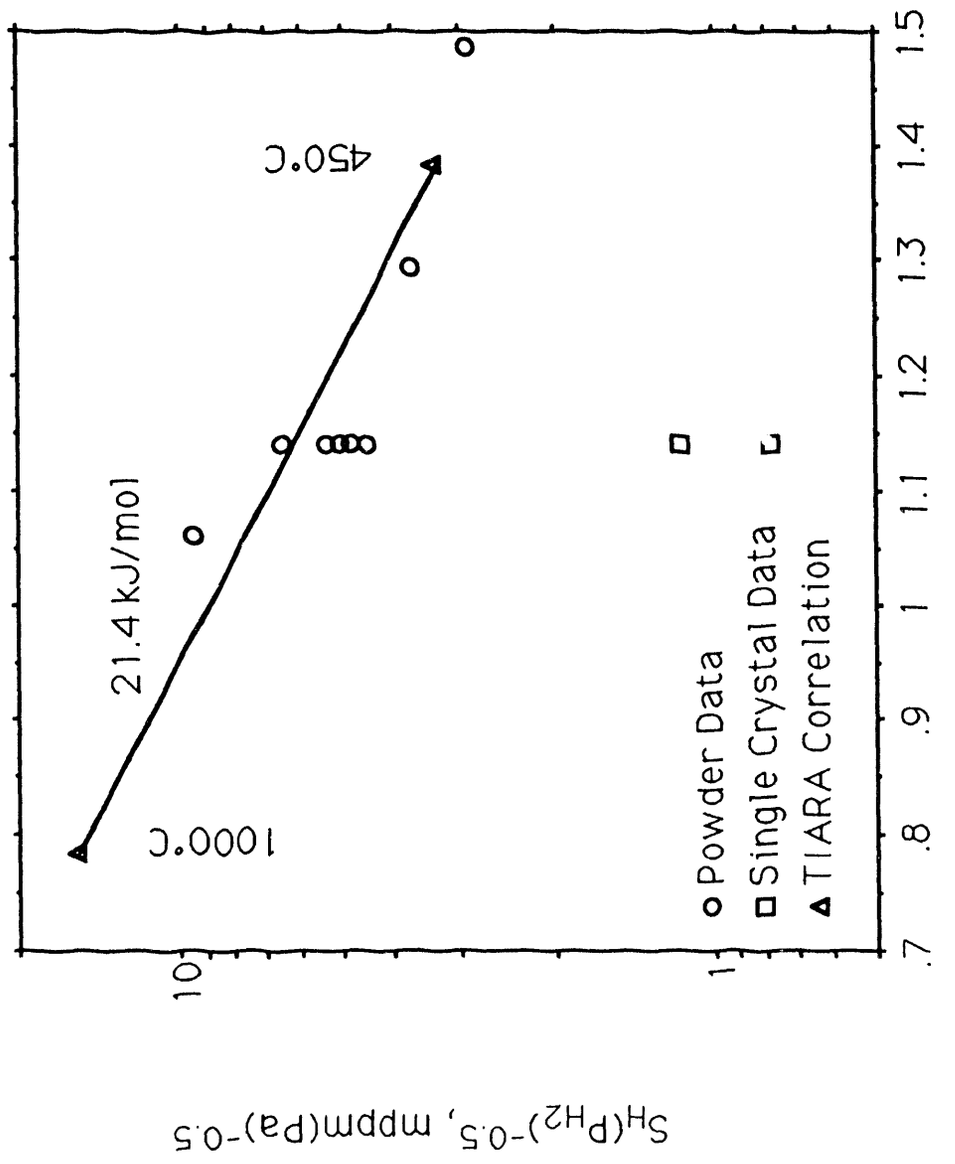

Fig. 4. Correlation vs. data for normalized H solubility in Li_2O.

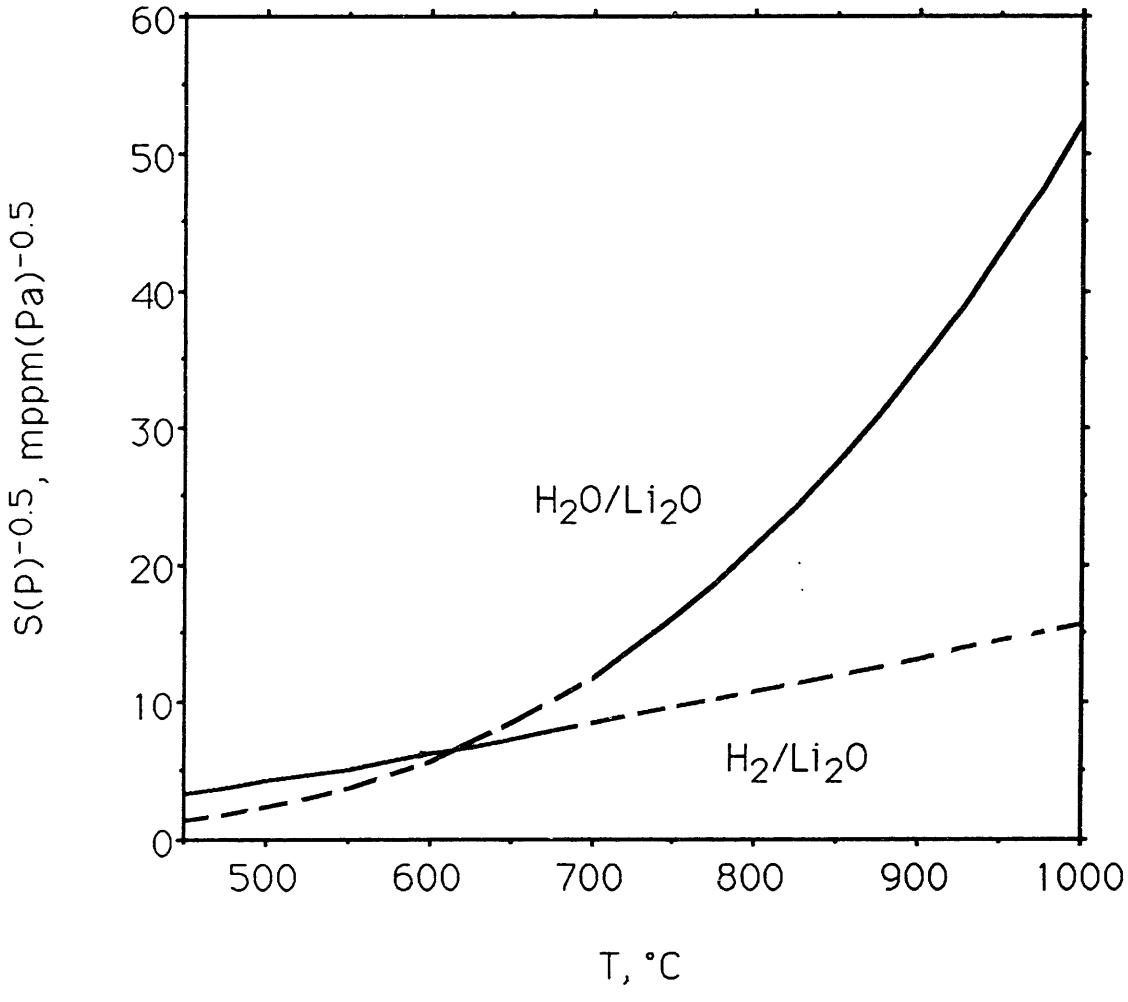

Fig. 5. Correlations for normalized solubility of hydrogen isotopes in Li_2O.

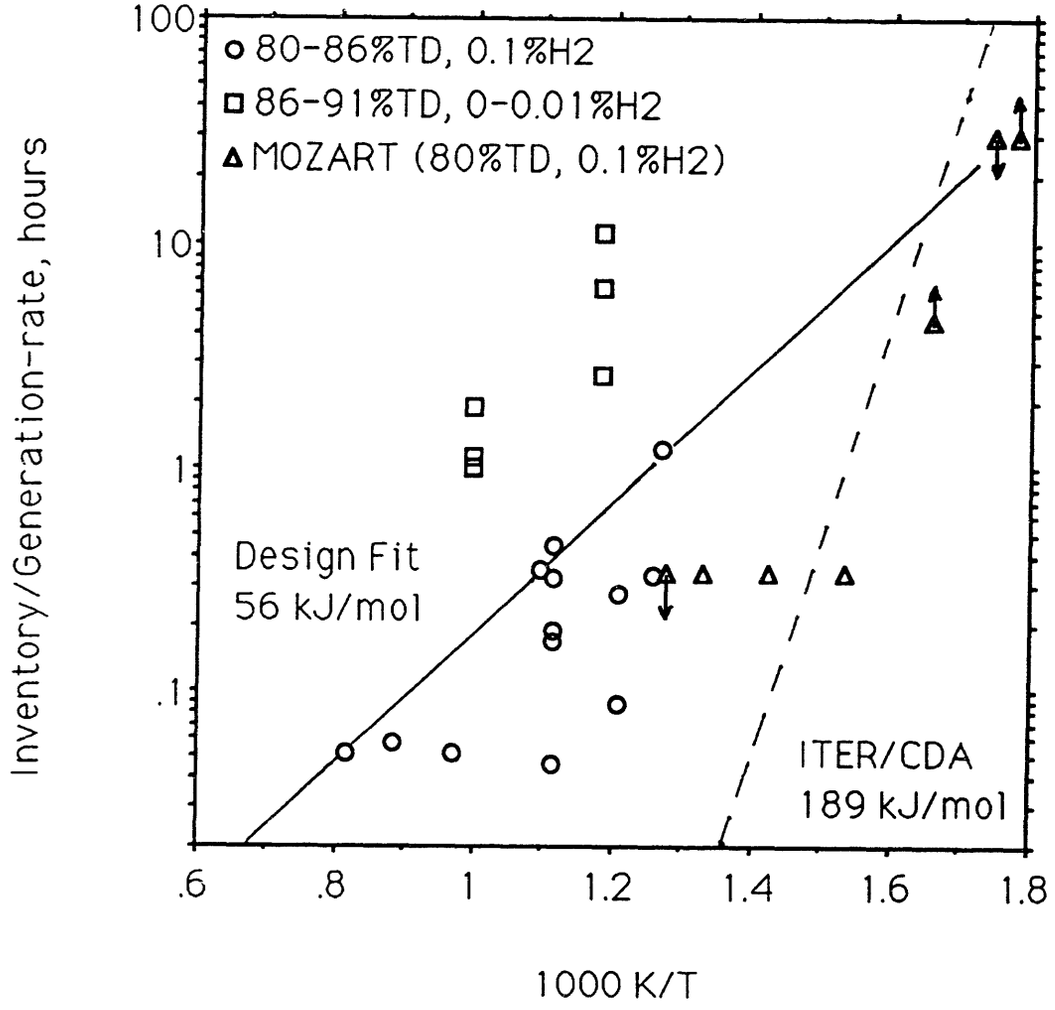

Fig. 6. Tritium residency times determined from Li_2O inventory and release data.

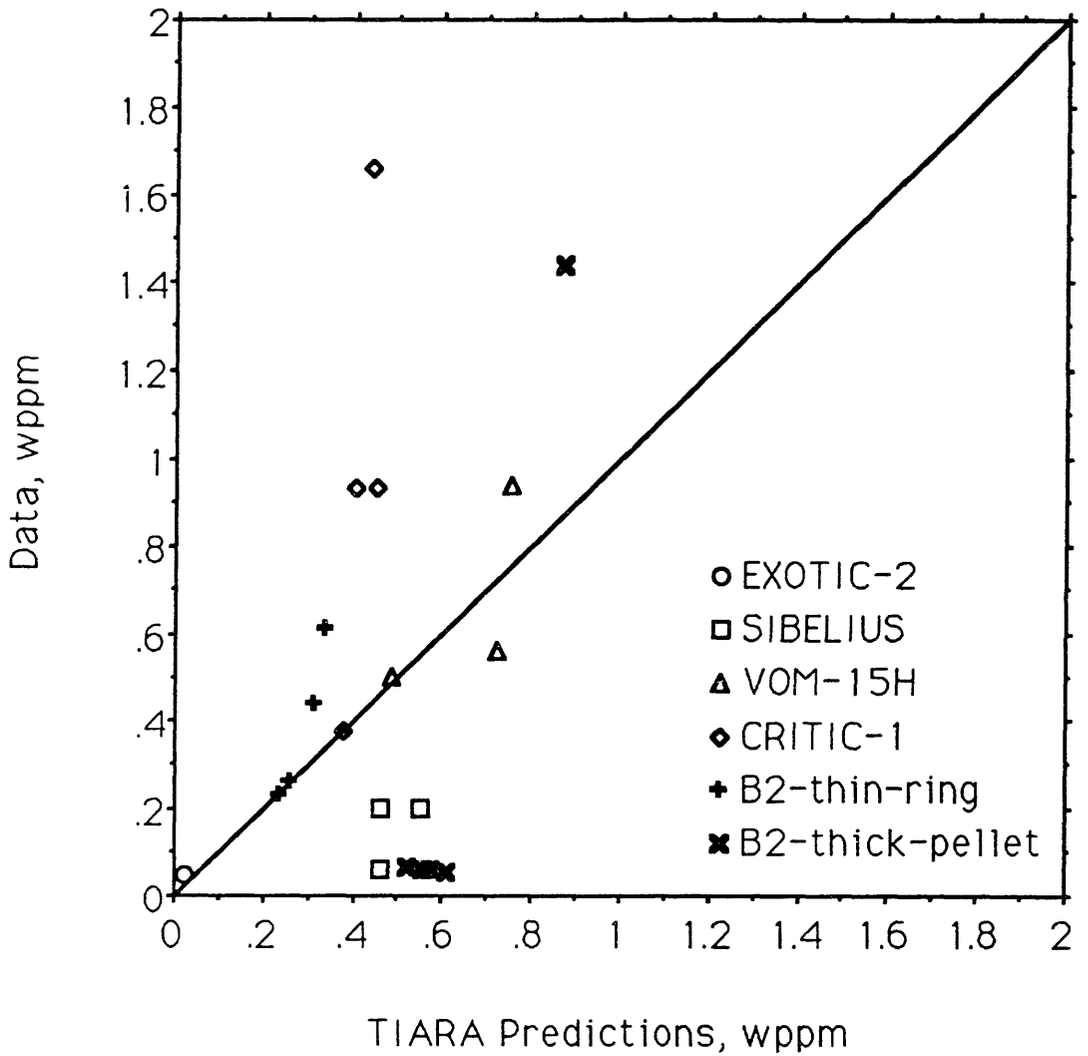

Fig. 7. TIARA validation to tritium inventory data for in-reactor purge-flow tests.

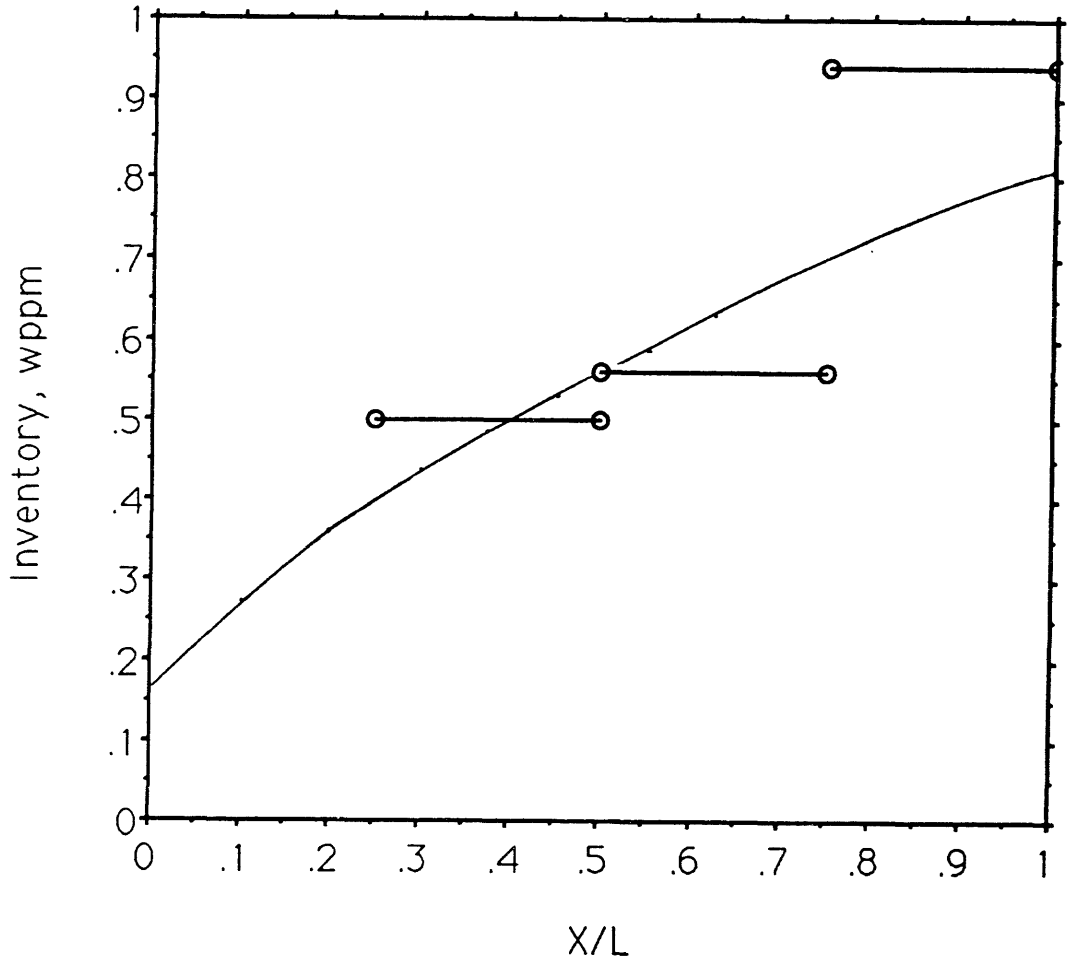

Fig. 8a. Tritium inventory axial profile prediction vs. data for VOM-15H.

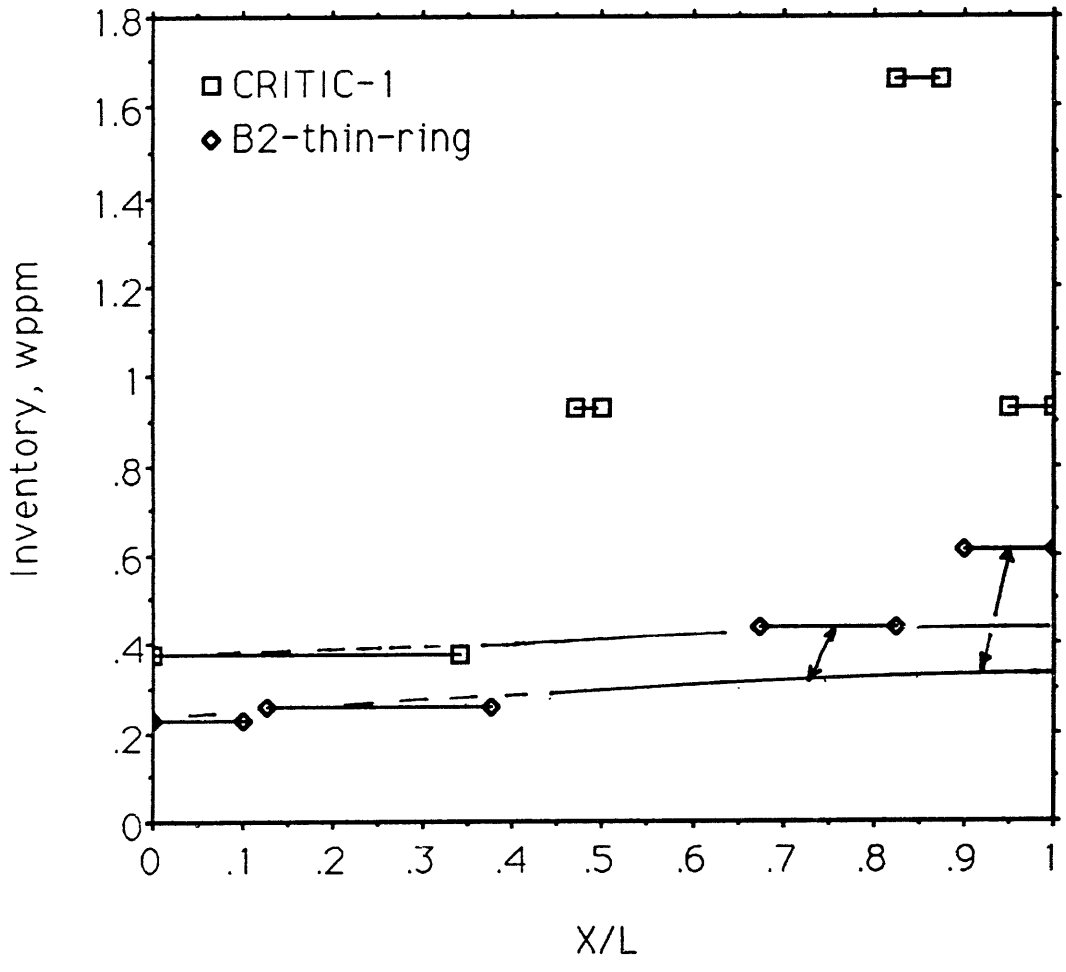

Fig. 8b. Tritium inventory axial profile predictions vs. data for CRITIC–1 and BEATRIX–2 (thin ring).

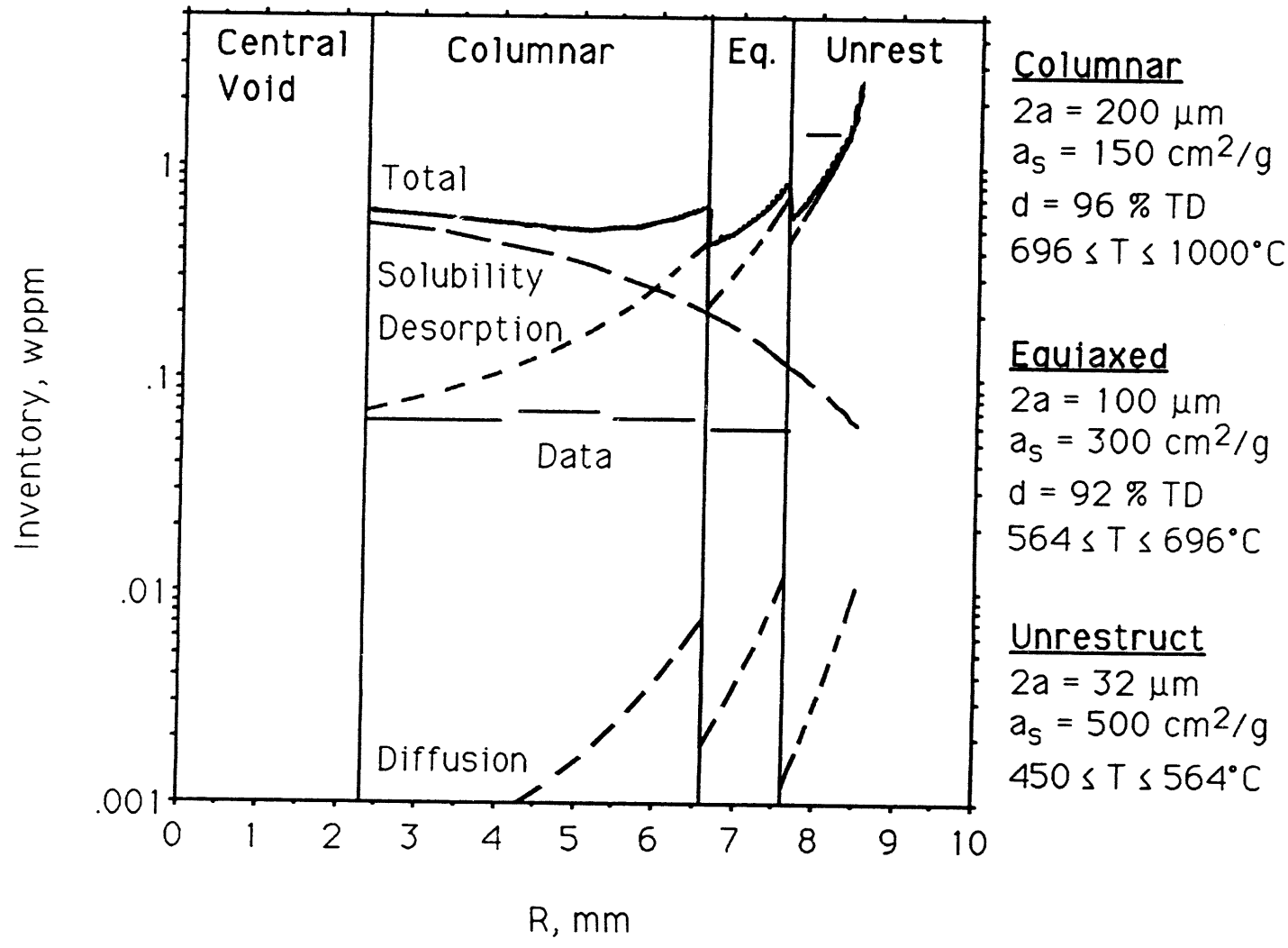

Fig. 9. Radial inventory profile prediction vs. data for BEATRIX–2 (thick pellet)

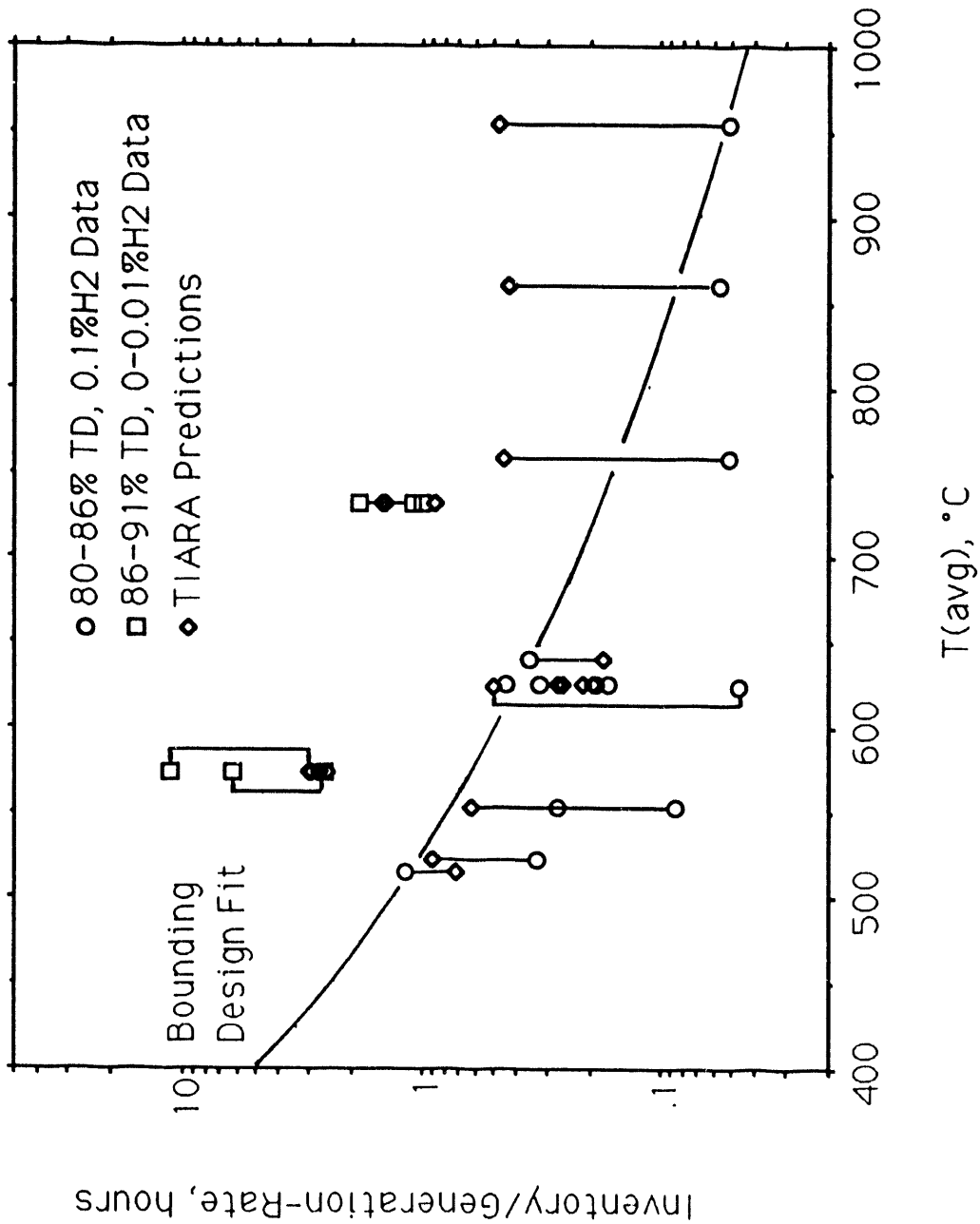

Fig. 10. Comparison of TIARA and design correlation to data for tritium residency times.

DATE
FILMED
6/23/94
END